Letter

Measurements of ion-electron energy-transfer cross section in high-energy-density plasmas

P. J. Adrian,[1] R. Florido,[2] P. E. Grabowski,[3] R. Mancini,[4] B. Bachmann,[3] L. X. Benedict,[3] M. Gatu Johnson,[1] N. Kabadi,[1] B. Lahmann,[1] C. K. Li,[1] R. D. Petrasso,[1] H. G. Rinderknecht,[5] S. P. Regan,[5] F. H. Séguin,[1] R. L. Singleton, Jr.,[6,7] H. Sio,[3] G. D. Sutcliffe,[1] H. D. Whitley,[3] and J. A. Frenje[1]

[1]*Plasma Science and Fusion Center, Massachusetts Institute of Technology, Cambridge, Massachusetts 02139, USA*
[2]*iUNAT, Departamento de Física, Universidad de Las Palmas de Gran Canaria, 35017 Las Palmas de Gran Canaria, Spain*
[3]*Lawrence Livermore National Laboratory, Livermore, California 94550, USA*
[4]*Department of Physics, University of Nevada, Reno, Reno, Nevada 89557, USA*
[5]*Laboratory for Laser Energetics, University of Rochester, Rochester, New York 14623, USA*
[6]*SavantX Research Center, Santa Fe, New Mexico 87501, USA*
[7]*School of Mathematics, University of Leeds, Leeds LS2 9JT, United Kingdom*

(Received 22 July 2021; revised 18 January 2022; accepted 2 September 2022; published 8 November 2022)

We report on measurements of the ion-electron energy-transfer cross section utilizing low-velocity ion stopping in high-energy-density plasmas at the OMEGA laser facility. These measurements utilize a technique that leverages the close relationship between low-velocity ion stopping and ion-electron equilibration. Shock-driven implosions of capsules filled with D ^{3}He gas doped with a trace amount of argon are used to generate densities and temperatures in ranges from 1×10^{23} to 2×10^{24} cm^{-3} and from 1.4 to 2.5 keV, respectively. The energy loss of 1-MeV DD tritons and 3.7-MeV D ^{3}He alphas that have velocities lower than the average velocity of the thermal electrons is measured. The energy loss of these ions is used to determine the ion-electron energy-transfer cross section, which is found to be in excellent agreement with quantum-mechanical calculations in the first Born approximation. This result provides an experimental constraint on ion-electron energy transfer in high-energy-density plasmas, which impacts the modeling of alpha heating in inertial confinement fusion implosions, magnetic-field advection in stellar atmospheres, and energy balance in supernova shocks.

DOI: 10.1103/PhysRevE.106.L053201

Obtaining a fundamental understanding of ion-electron energy transfer is an essential prerequisite for correctly describing the evolution of high-energy-density (HED) and inertial confinement fusion (ICF) plasmas. This is especially important in scenarios where ions and electrons are differentially heated and the ion-electron collision frequency is on the order of the plasma-evolution timescale. Scenarios where ion-electron collisions play an important role are shock waves where ion-electron collisions dictate the plasma profiles [1], laser ablation where electron heating is driven by inverse bremsstrahlung [2], magnetic-field advection where fields are reorganized by the Nernst effect [3], alpha heating in ICF implosions where ion-electron collisions mediate the nuclear-burn wave [4–6], the core collapse of supernovae where ion-electron collisions impact the magnetic Raleigh-Taylor instability [7], and shocks in supernova remnants [8–10]. To understand the dynamics of these plasmas, models and theories of ion-electron collisions must be accurate over a wide range of plasma conditions. While extensive theoretical work has been done to describe ion-electron collisions [11–32], there is a paucity of experimental methodologies to test these theories. The lack of data prevents model validation and increases the level of uncertainty in simulations of HED plasmas [33]. We are aware of two experiments that have made an attempt to study ion-electron energy transfer at high density (greater than 10^{23} cm^{-3}) and temperature (greater than 1 keV) in implosions [34,35]. However, the implosion dynamics [34], three-dimensional asymmetries [36], and thermal gradients [37] severely complicated their interpretation of the time-integrated results.

In this Letter, we report on precision measurements of the ion-electron energy-transfer cross section in HED plasmas using a measurement technique that avoids the complications in previous work. Our experimental methodology utilizes the stopping power of nearly monoenergetic ions below the Bragg peak for the determination of the Coulomb logarithm (proportional to the ion-electron energy-transfer cross section) for electron densities n_e and temperatures T_e in the ranges from 1×10^{23} to 2×10^{24} cm^{-3} and from 1.4 to 2.5 keV, respectively.

Ion-electron equilibration depends on the ion-electron energy-transfer cross section of thermal ions scattering off thermal electrons, while the ion stopping power depends on the momentum-transfer cross section of arbitrarily fast ions interacting with the thermal electrons. When the velocity of the projectile ions (V_i) is lower than the average velocity of the thermal electrons (V_{Te}), i.e., $V_i < V_{Te}$, the cross sections for energy and momentum transfer are trivially related. In fact, it has been shown previously [14,16,17,28,38] that for $V_i < V_{Te}$ the ion stopping is expressed as

$$\frac{dE}{dx} = -\nu_{ie}^{p} m_i V_i(x), \tag{1}$$

TABLE I. Experimental implosion parameters and key plasma conditions for inferring an experimental Coulomb logarithm $\ln\Lambda_{\rm expt}$.

	Fill	Laser [70]	Bang times [64] (ps)			Yields [65]		Temperature (keV)		$\langle n_e\rangle$ [68]	$\langle n_e L\rangle$ [68]	$\Delta E_i/Z_i^2$ (MeV) [66]		
Shot	$D_2/^3$He/Ar (atm)	(kJ)	DD	D ^{3}He	X ray	DD	D ^{3}He	$\langle T_i\rangle$ [67]	$\langle T_e\rangle$ [68]	($\times10^{23}$ cm^{-3})	($\times10^{21}$ cm^{-2})	DD triton [69]	D ^{3}He-α	$\ln\Lambda_{\rm expt}$
78608	5.0/11.3/0.10	7.4	1190	1220		2.0×10^9	1.4×10^9	5.9 ± 0.3	1.4 ± 0.1	21 ± 4.2	5.0 ± 1.0	0.28	0.47	2.9 ± 0.8
78609	5.0/11.7/0.11	7.2	1217	1240		1.6×10^9	1.1×10^9	5.6 ± 0.3	1.4 ± 0.1	21 ± 4.2	5.0 ± 1.0	0.35	0.51	3.4 ± 1.1
78611	5.0/11.3/0.10	6.4	1327	1360		5.4×10^8	6.3×10^8	4.8 ± 0.3	1.6 ± 0.2	11 ± 4.5	4.5 ± 0.9		0.42	4.1 ± 1.1
78612	5.0/11.5/0.12	6.1	1309	1334		6.2×10^8	5.2×10^8	5.0 ± 0.3	1.6 ± 0.2	11 ± 4.5	4.5 ± 0.9		0.42	4.0 ± 1.1
75694	3.0/6.8/0.15	12.0	1065	1100	1140	1.5×10^{10}	1.1×10^{10}	8.8 ± 0.3	2.8 ± 0.3	6.6 ± 1.0	4.1 ± 0.4	0.19	0.28	5.8 ± 1.4
75695	3.0/6.7/0.14	9.9	1095	1163	1215	1.1×10^{10}	5.9×10^9	7.8 ± 0.3	2.3 ± 0.2	4.6 ± 0.7	4.5 ± 0.5	0.30	0.41	5.1 ± 1.5
75698	3.0/6.0/0.14	9.9	1110	1173	1220	1.1×10^{10}	5.3×10^9	7.6 ± 0.3	2.1 ± 0.2	4.8 ± 0.7	4.3 ± 0.4	0.25	0.41	5.3 ± 1.4
75699	3.0/6.7/0.12	8.1	1195	1254	1292	7.3×10^9	2.3×10^9	6.6 ± 0.3	1.9 ± 0.2	3.9 ± 0.6	3.9 ± 0.4	0.28	0.41	5.4 ± 1.5
75700	3.0/6.7/0.12	8.0	1185	1258	1300	6.6×10^9	2.1×10^9	7.0 ± 0.3	1.9 ± 0.2	3.8 ± 0.6	4.2 ± 0.4	0.24	0.34	4.4 ± 1.2
75701	3.0/6.5/0.15	6.6	1330	1360	1430	2.7×10^9	3.2×10^8	4.6 ± 0.3	1.8 ± 0.2	5.1 ± 0.8	3.2 ± 0.3	0.34	0.45	4.2 ± 1.2
75702	3.0/7.1/0.14	6.3	1350	1398	1525	2.4×10^9	2.7×10^8	4.5 ± 0.3	1.4 ± 0.2	3.8 ± 0.8	5.2 ± 0.3	0.27	0.40	3.9 ± 1.1

where m_i is the mass of the ion and ν_{ie}^p is the momentum-transfer frequency given by

$$\nu_{ie}^p = \frac{4\pi}{3}\sqrt{\frac{2}{\pi}}\sqrt{\frac{m_e}{m_i^2}}Z_i^2 e^4 \frac{n_e}{T_e^{3/2}}\ln\Lambda \tag{2}$$

for a weakly coupled and nondegenerate plasma (CGS units). Here $\ln\Lambda$ is the Coulomb logarithm, m_e is the electron mass, and Z_i is the ion charge. Similarly, the temperature relaxation can be expressed as

$$\frac{dT_i}{dt} = -\nu_{ie}^E(T_i - T_e), \tag{3}$$

where T_i is the ion temperature and ν_{ie}^E is the energy-transfer frequency. The energy- and momentum-transfer frequencies are related as $\nu_{ie}^E = 2\nu_{ie}^p$.

A tracer particle moving with $V_i < V_{Te}$ loses energy by an amount [62]

$$\Delta E_i = m_i V_i \langle\nu_{ie}^p\rangle - \tfrac{1}{2}m_i\langle\nu_{ie}^p\rangle^2, \tag{4}$$

where $\langle\nu_{ie}^p\rangle = \int \nu_{ie}^p dx$ is the path-integrated collision frequency. Thus, the energy-transfer cross section (or $\ln\Lambda$) governing both the low-velocity stopping power and the ion-electron equilibration process is determined from measurements of ΔE_i, n_e, and T_e.

The connection between ion stopping power and ion-electron equilibration has been exploited theoretically. First, the T-matrix formalism for calculating the collision term in the treatment of stopping power by Gericke *et al.* [39] was borrowed to calculate temperature relaxation [14]. Second, Bernstein *et al.* [40] utilized this connection to investigate the effects of strong coupling on temperature relaxation through MD simulations. This work is an experimental effort to utilize this connection.

The classical description of ion-electron energy transfer was first described by Landau [11] and Spitzer [12]. In the Landau-Spitzer (LS) formalism, a Coulomb logarithm is included to regularize the integration of the ion-electron differential cross section for elastic scattering, which diverges due to improper treatment of the Coulomb potential. The Coulomb logarithm for a classical plasma is $\ln(\mathcal{C}_{\rm cl}\lambda_{\rm De}/\lambda_L)$, where $\lambda_{\rm De} = \sqrt{T_e/4\pi n_e e^2}$ is the Debye length, $\lambda_L = Z_i e^2/T_e$ is the Landau length, and $\mathcal{C}_{\rm cl}$ is a correction factor derived from the weak-scattering approximation [22]. On the basis of calculations and simulations, $\mathcal{C}_{\rm cl} = 0.765$ for classical plasmas [16,18,41]. This expression captures the screening physics for large impact parameters and local field corrections at the classical distance of closest approach. The LS theory breaks down because quantum diffraction, electron degeneracy, and strong coupling are not considered. In recent years, various theories and computational tools have been developed to address the impact of quantum effects. The Gericke-Murillo-Schlanges (GMS) theory [14] was derived by using a quantum Boltzmann collision operator combined with a T-matrix calculation of the differential cross section for elastic scattering. This theory, which is widely used in radiation-hydrodynamics codes for modeling of ICF and HED plasmas, captures strong coupling and quantum-diffraction effects in the scattering process, but neglects aspects of the dynamical screening of the ion-electron interaction. This paper uses the GMS6 result, which is a fit to the full T-matrix result and is the sixth entry in Table I of Ref. [14]. The quantum Lenard-Balescu formalism (QLB) was developed for weakly coupled plasmas to treat ion-electron interactions with a linear-response formalism [15,22,25,26,28,31]. The QLB theory includes dynamical screening through a wave-vector- and frequency-dependent dielectric function evaluated in the random-phase approximation (RPA) and considers Pauli blocking and quantum diffraction [23]. This theory has an analytic expression for calculating the ion-electron energy-transfer cross section derived in Ref. [31]. The quantum Landau–Fokker-Planck (QFP) theory [28] is the QLB result but ignores dynamic screening in the RPA dielectric response function. Brown *et al.* used dimensional continuation to regularize the divergence in the integral of the ion-electron energy-transfer cross section [16,17]. This theory includes the modeling of quantum diffraction and electron degeneracy. Finally, an analytical expression for the ion-electron cross section was computed using the first Born approximation to calculate the scattering amplitudes of electrons interacting with a Debye screened potential [42]. All five theories have been implemented in various hydrodynamics codes to simulate HED plasmas [43,44].

Central to this discussion is that the GMS, QLB, QFP, and Brown-Preston-Singleton (BPS) theories differ in the computation of the ion-electron Coulomb logarithm

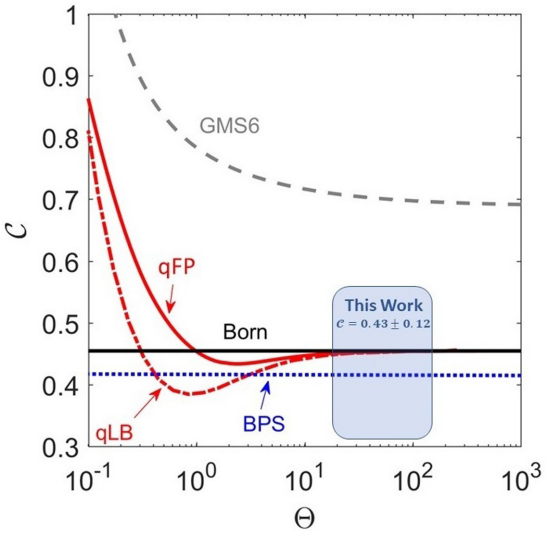

FIG. 1. Parameter $\mathcal{C}$ as a function of Θ for the QLB (red dash-dotted line), QFP (red solid line), BPS (blue dotted line), and GMS6 (gray dashed line) theories evaluated at the $T_e = 2$ keV and $Z_i = 1$. Also shown is $\mathcal{C}$ computed in the first Born approximation (black solid line). As discussed in the text, this work probes $\Theta = 20$–100, where $\mathcal{C}$ is insensitive to the plasma conditions and thus has a very weak dependence on Z_i. The blue box represents the constraints on $\mathcal{C}$ obtained from measurements detailed in this work. Evaluations of the Coulomb logarithm for each theory are found in the Supplemental Material [45].

(ion-electron energy-transfer cross section). Figure 1 illustrates the differences by fitting each theory to the form of $\ln\Lambda$ as $\ln(\mathcal{C}\lambda_{\rm De}/\lambda_Q)$, where $\lambda_Q = \sqrt{\hbar^2/8m_eT_e}$ is proportional to the de Broglie wavelength and $\mathcal{C}$ is a correction factor. Figure 1 displays $\mathcal{C}$ as a function of the degeneracy parameter Θ, which is the ratio of T_e to the Fermi energy. For the various theories, $\mathcal{C}$ is independent of plasma conditions at the conditions relevant to this work, with the GMS theory predicting $\mathcal{C} = 0.7$ and the QLB and QFP theories predicting 0.45. Also shown in Fig. 1 is the line $\mathcal{C} = 0.45$, which is predicted by the first Born approximation (black solid line) [42]. The BPS theory has a weak dependence on the electron temperature T_e. The QLB, QFP, and BPS theories asymptote to the first Born approximation at high Θ and T_e.

This work utilized the established methodology for precision ion stopping power measurements [46,47] at the OMEGA laser facility [48]. Thin-shell glass capsules filled with D ^{3}He and trace amounts of argon gas were imploded. The capsule initial conditions and the laser parameters are summarized in Table I. The laser intensity on the capsule was kept below the two-plasmon-decay threshold to avoid capsule charging that would affect these measurements [51,52]. As the laser ablates the glass shell, it drives a strong shock through the D ^{3}He gas, which rebounds at the center of the implosion causing DD and D ^{3}He fusion reactions. These reactions generate 1-MeV DD tritons, 3.7-MeV D ^{3}He alphas, 3.0-MeV DD protons, and 14.7-MeV D ^{3}He protons. As the velocity of the DD tritons (approximately 5×10^6 m/s) and D ^{3}He alpha (approximately 9×10^6 m/s) are below V_{Te} (approximately 1.8×10^7 m/s at $T_e = 2$ keV) in these experiments, these low-velocity ions were used to probe the ion-electron energy-transfer cross section. Four measurements essential to this effort were (i) measurements of the DD and D ^{3}He fusion-product spectra, (ii) measurements of the DD and D ^{3}He reaction histories, and measurements of (iii) $T_e(r,t)$ and (iv) $n_e(r,t)$. The fusion-product spectra were measured with the charged particle spectrometers [53]. The energy loss ΔE of each fusion product was determined by subtracting the measured mean energy from the birth energy predicted by Ballabio *et al.* [54] using the measured average ion temperature $\langle T_i \rangle$ shown in Table I. An example of measured DD-triton and D ^{3}He-alpha spectra and associated ΔE are shown in Figs. 2(a) and 2(b). The measured $\Delta E_i/Z_i^2$ for the DD triton and D ^{3}He alpha are given in Table I.

The DD and D ^{3}He reaction histories were measured simultaneously with the particle x-ray temporal diagnostic (PXTD) [49] and an example of resulting data is show in Fig. 2(c). There is a systematic timing difference between the DD and D ^{3}He reaction histories for all shots presented in this paper, indicating that the DD-triton and D ^{3}He-alpha sample different plasma conditions. These data together with simulations are used to account for the effect of evolving plasma conditions that have an impact on the measured ΔE, as previously noted by Frenje *et al.* [47]. The DD and D ^{3}He

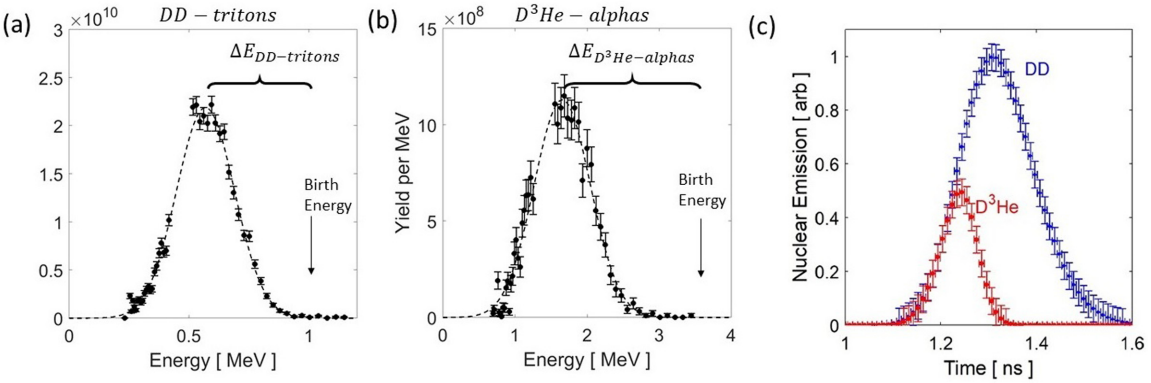

FIG. 2. Example of measured (a) DD-triton and (b) D ^{3}He-alpha spectra (shot 78 609). The birth energy and ΔE are indicated. (c) Measured DD and D ^{3}He nuclear-reaction histories.

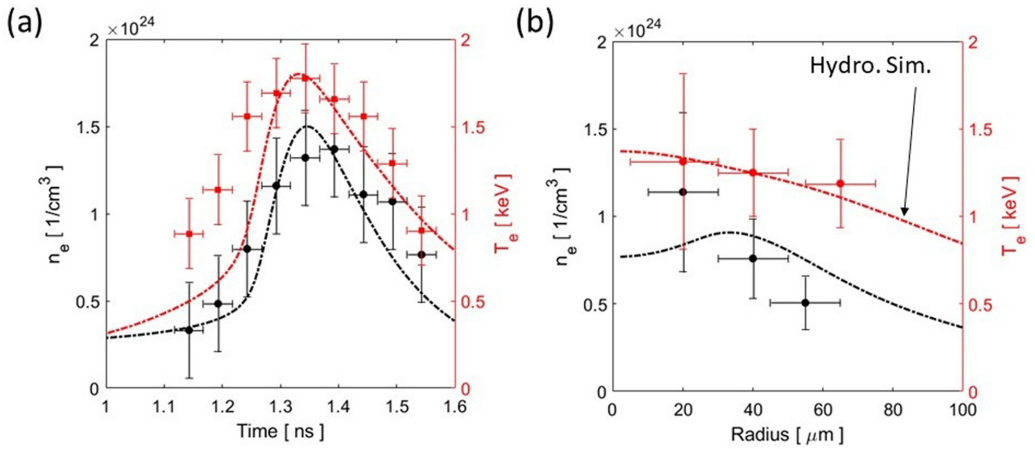

FIG. 3. Example of measured (data points) and hydrosimulated (dash-dotted line) plasma conditions for shot 78 609 for (a) $n_e(t)$ and $T_e(t)$ and (b) $T_e(r)$ and $n_e(r)$. Hydrosimulated plasma conditions were scaled with a constant multiplier.

emission profiles were imaged using the particle core imaging system (PCIS)[55].

Argon He-β, Ly-β, and Ly-γ line emissions were measured using a time-resolving x-ray spectrometer to infer $n_e(t)$ and $T_e(t)$ [56,57]. Example data are shown in Fig. 3(a). These data clearly demonstrate that n_e increases about 20% from peak D ^{3}He emission to peak DD emission, information that is necessary when correcting the measured ΔE of the D ^{3}He alpha.

Absolute $n_e(r)$ and $T_e(r)$ profiles were diagnosed with the multimonochromatic imager through measurements of the spatial distribution of argon line emission [58]. Example profiles are shown in Fig. 3(b). These profiles, which were integrated over a time gate of 100 ps during the x-ray emission period, were used to scale the magnitude of the HYADES [59] simulated profiles. The comparison between the measured and simulated profiles for shot 78 609 is also shown in Fig. 3(b).

A one-dimensional code was developed and used to transport the DD triton and D ^{3}He alpha through the well-characterized evolving density and temperature profiles. In the code, the source characteristics of these two fusion products were determined from the PCIS and PXTD data. At each step (in time and space) the fusion products felt the local friction computed from the Maynard-Deutsch stopping power model [60,61]. The fractional energy lost was also computed and was used to compute the dE/dx-weighted plasma conditions $\langle T_e\rangle$, $\langle n_e\rangle$, and $\langle n_e L\rangle$ at each step (for more information see the Supplemental Material [45]). These parameters are presented in Table I for every shot. The quantities represent the average conditions that particles probe accounting for the evolving plasma conditions.

The $\langle T_e\rangle$ and $\langle n_e\rangle$ values were used to generate BPS-predicted $\Delta E_i/Z_i^2$ curves versus V_i/V_{Te} that are contrasted to the measured data for all four fusion products shown in Fig. 4. The comparison clearly indicates that the BPS theory does an excellent job describing the measured energy loss,[63] as already demonstrated in Ref. [47]. Figure 4 also displays the linear-drag model computed from Eq. (2) (dashed line). The measured ΔE_i of the DD triton and D ^{3}He alpha were used to determine $\ln\Lambda_{\rm expt}$ from the linear drag model [Eqs. (2) and (4)]. This was done for every shot shown in Table I. Since $\mathcal{C}$ is expected to be constant at these plasma conditions, $\mathcal{C}$ is fit to all measurements of $\ln\Lambda_{\rm expt}$, where $\langle n_e\rangle$ and $\langle T_e\rangle$ were used to calculate $\lambda_{\rm De}$ and λ_Q. The result is shown in Fig. 5. The best fit yields $\mathcal{C} = 0.43 \pm 0.12$, which minimizes $\ln\Lambda_{\rm expt} - \ln(\mathcal{C}\lambda_{\rm De}/\lambda_Q)$. This result is consistent with the QLB, QFP, and BPS predictions, indicating that the small-angle scattering is well described by the first Born approximation of the elastic scattering cross section. The measurements are inconsistent with the GMS6 model, which is a fit to T-matrix calculations over a wide parameter space. Subsequently, our data imply that the fitted formulas for the T-matrix results should be revisited for accuracy.

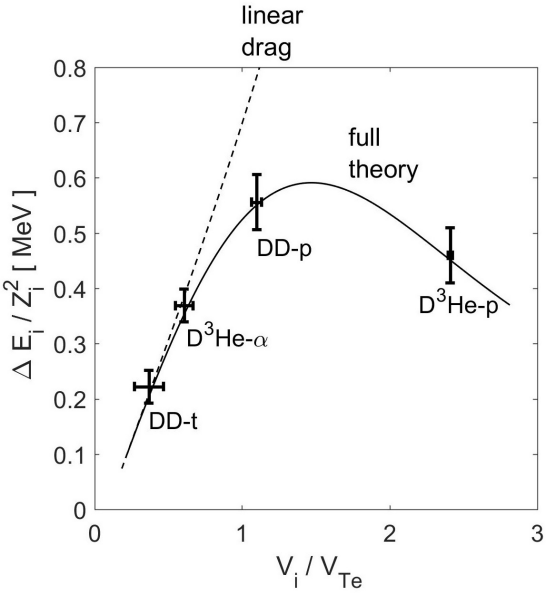

FIG. 4. Example of measured ΔE (normalized by Z_i^2) versus ion velocity V_i, normalized by electron thermal velocity V_{Te} (shot 78 209). The black solid curve is the energy loss predicted by the BPS theory for the plasma conditions given in Table I. The black dashed line represents the energy loss determined from the linear drag model when $V_i < V_{Te}$ [see Eq. (4)].

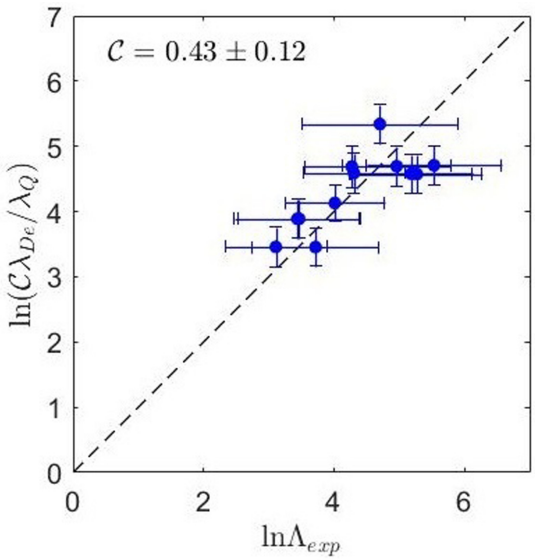

FIG. 5. Coulomb logarithm $\ln(\mathcal{C}\lambda_{\mathrm{De}}/\lambda_Q)$ versus measured $\ln\Lambda_{\mathrm{expt}}$. The measurements of $\langle n_e\rangle$ and $\langle T_e\rangle$ were used to calculate λ_{De} and λ_Q. The value of $\mathcal{C}$, which minimizes $\ln\Lambda_{\mathrm{expt}} - \ln(\mathcal{C}\lambda_{\mathrm{De}}/\lambda_Q)$, was determined to be 0.43 ± 0.12.

In summary, high-precision measurements of ion-electron energy-transfer cross section in a weakly coupled and nondegenerate HED plasma were conducted using a technique based on low-velocity ion stopping power measurements. The measurements determined the Coulomb logarithm and showed that ion-electron energy transfer in this regime is well described by QLB, QFP, or BPS theories. The applicability of these theories extends further than the scope of the measurements, as they are expected to be accurate for nondegenerate ($\Theta \gg 1$), weakly coupled ($\Gamma \ll 0.1$) plasmas where $\lambda_L/\lambda_Q \ll 1$. Our results are relevant to the energy balance in ICF hot spots ($n_e \sim 10^{24}$–10^{26} cm^{-3} and $T_e \sim$ 3–5 keV) and laser ablation ($n_e < 10^{21}$ cm^{-3} and $T_e \sim$ 1–3 keV), as well as astrophysical systems such as supernova shocks ($n_e < 1$ cm^{-3} and $T_e > 0.1$ keV). Simulations that model plasmas in these regimes should implement the ion-electron energy-transfer cross section of the QLB, QFP, or BPS theory to provide the most accurate ion-electron energy transport. In future experiments, the low-velocity ion stopping technique should be leveraged to probe ion-electron energy exchange in more degenerate and strongly coupled plasmas where the QLB, QFP, and BPS models begin to disagree, as shown in Fig. 1.

This work was supported by the U.S. Department of Energy under Grant No. DE-NA0003868, the Laboratory for Laser Energetics under Grant No. 417532G/UR FAO GR510907, Lawrence Livermore National Laboratory under Contract No. DE-AC52-07NA27344, and the National Laser Users' Facility under Grant No. DE-NA0003938. P.J.A. was supported by Grant No. DE-NA0003960. R.F. was supported by Grants No. GOB-ESP2019-13 (ULPGC) and No. PID2019-108764RB-I00 (MICNN, Spain).

[1] Y. B. Zel'dovich and Y. P. Raizer, *Physics of Shock Waves and High-Temperature Hydrodynamic Phenomena* (Academic, New York, 1967).
[2] S. Atzeni and J. Meyer-ter Vehn, *The Physics of Inertial Fusion: Beam Plasma Interaction, Hydrodynamics, Hot Dense Matter* (Oxford University Press, Oxford, 2004).
[3] M. J.-E. Manuel *et al.*, Phys. Plasmas **20**, 056301 (2013).
[4] C.-K. Li and R. D. Petrasso, Phys. Rev. Lett. **70**, 3063 (1993).
[5] H. Brysk, P. M. Campbell, and P. Hammerling, Plasma Phys. **17**, 473 (1975).
[6] A. B. Zylstra and O. A. Hurricane, Phys. Plasmas **26**, 062701 (2019).
[7] M. J.-E. Manuel *et al.*, Phys. Plasmas **22**, 056305 (2015).
[8] P. Ghavamian, S. J. Schwartz, J. Mitchell, A. Masters, and J. M. Laming, Space Sci. Rev. **178**, 633 (2013).
[9] M. van Adelsberg, K. Heng, R. McCray, and J. C. Raymond, Astrophys. J. **689**, 1089 (2008).
[10] J. Vink, S. Broersen, A. Bykov, and S. Gabici, Astron. Astrophys. **579**, A13 (2015).
[11] L. D. Landau, J. Exp. Theor. Phys. **7**, 203 (1937).
[12] L. Spitzer, Jr., *Physics of Fully Ionized Gases*, 2nd ed. (Wiley Interscience, New York, 1962).
[13] M. W. C. Dharma-wardana and F. Perrot, Phys. Rev. E **58**, 3705 (1998).
[14] D. O. Gericke, M. S. Murillo, and M. Schlanges, Phys. Rev. E **65**, 036418 (2002).
[15] D. O. Gericke, J. Phys.: Conf. Ser. **11**, 111 (2005).
[16] L. S. Brown, D. L. Preston, and R. L. Singleton, Jr., Phys. Rep. **410**, 237 (2005).
[17] L. S. Brown and R. L. Singleton, Phys. Rev. E **76**, 066404 (2007).
[18] G. Dimonte and J. Daligault, Phys. Rev. Lett. **101**, 135001 (2008).
[19] G. Gregori and D. O. Gericke, Europhys. Lett. **83**, 15002 (2008).
[20] J. N. Glosli, F. R. Graziani, R. M. More, M. S. Murillo, F. H. Streitz, M. P. Surh, L. X. Benedict, S. Hau-Riege, A. B. Langdon, and R. A. London, Phys. Rev. E **78**, 025401(R) (2008).
[21] B. Jeon, M. Foster, J. Colgan, G. Csanak, J. D. Kress, L. A. Collins, and N. Grønbech-Jensen, Phys. Rev. E **78**, 036403 (2008).
[22] J. Daligault and G. Dimonte, Phys. Rev. E **79**, 056403 (2009).
[23] J. Vorberger and D. O. Gericke, Phys. Plasmas **16**, 082702 (2009).
[24] F. R. Graziani *et al.*, High Energy Density Phys. **8**, 105 (2012).
[25] L. X. Benedict *et al.*, Phys. Rev. E **86**, 046406 (2012).
[26] D. A. Chapman, J. Vorberger, and D. O. Gericke, Phys. Rev. E **88**, 013102 (2013).
[27] *Frontiers and Challenges in Warm Dense Matter*, edited by F. Graziani, M. P. Desjarlais, R. Redmer, and S. B. Trickey, Lecture Notes in Computational Science and Engineering (Springer International, Cham, 2014).
[28] J. Daligault, Phys. Plasmas **23**, 032706 (2016).
[29] L. G. Stanton and M. S. Murillo, Phys. Rev. E **93**, 043203 (2016).
[30] L. X. Benedict *et al.*, Phys. Rev. E **95**, 043202 (2017).

[31] C. R. Scullard, S. Serna, L. X. Benedict, C. L. Ellison, and F. R. Graziani, Phys. Rev. E **97**, 013205 (2018).
[32] S. Rightley and S. D. Baalrud, Phys. Rev. E **103**, 063206 (2021).
[33] J. A. Gaffney, S. T. Brandon, K. D. Humbird, M. K. G. Kruse, R. C. Nora, J. L. Peterson, and B. K. Spears, Phys. Plasmas **26**, 082704 (2019).
[34] J. R. Rygg, J. A. Frenje, C. K. Li, F. H. Séguin, R. D. Petrasso, D. D. Meyerhofer, and C. Stoeckl, Phys. Rev. E **80**, 026403 (2009).
[35] C. L. Ellison *et al.*, Phys. Plasmas **25**, 072710 (2018).
[36] M. Gatu Johnson *et al.*, Phys. Plasmas **25**, 056303 (2018).
[37] H. D. Whitley *et al.*, High Energy Density Phys. **38**, 100928 (2021).
[38] D. O. Gericke, Laser Part. Beams **20**, 471 (2002).
[39] D. O. Gericke, M. Schlanges, and T. Bornath, Phys. Rev. E **65**, 036406 (2002).
[40] D. J. Bernstein, S. D. Baalrud, and J. Daligault, Phys. Plasmas **26**, 082705 (2019).
[41] T. Kihara and O. Aono, J. Phys. Soc. Jpn. **18**, 837 (1963).
[42] M. R. Zaghloul, M. A. Bourham, and J. M. Doster, Phys. Lett. A **268**, 375 (2000).
[43] B. Xu and S. X. Hu, Phys. Rev. E **84**, 016408 (2011).
[44] S. D. Bergeson, S. D. Baalrud, C. L. Ellison, E. Grant, F. R. Graziani, T. C. Killian, M. S. Murillo, J. L. Roberts, and L. G. Stanton, Phys. Plasmas **26**, 100501 (2019).
[45] See Supplemental Material at http://link.aps.org/supplemental/10.1103/PhysRevE.106.L053201 for details.
[46] J. A. Frenje, P. E. Grabowski, C. K. Li, F. H. Séguin, A. B. Zylstra, M. Gatu Johnson, R. D. Petrasso, V. Y. Glebov, and T. C. Sangster, Phys. Rev. Lett. **115**, 205001 (2015).
[47] J. A. Frenje *et al.*, Phys. Rev. Lett. **122**, 015002 (2019).
[48] T. R. Boehly *et al.*, Opt. Commun. **133**, 495 (1997).
[49] H. Sio *et al.*, Rev. Sci. Instrum. **87**, 11D701 (2016).
[50] V. Y. Glebov, C. Stoeckl, T. C. Sangster, S. Roberts, G. J. Schmid, R. A. Lerche, and M. J. Moran, Rev. Sci. Instrum. **75**, 3559 (2004).
[51] C. Stoeckl, R. E. Bahr, B. Yaakobi, W. Seka, S. P. Regan, R. S. Craxton, J. A. Delettrez, R. W. Short, J. Myatt, A. V. Maximov, and H. Baldis, Phys. Rev. Lett. **90**, 235002 (2003).
[52] D. G. Hicks *et al.*, Phys. Plasmas **7**, 5106 (2000).
[53] F. H. Séguin *et al.*, Rev. Sci. Instrum. **74**, 975 (2003).
[54] L. Ballabio, J. Källne, and G. Gorini, Nucl. Fusion **38**, 1723 (1998).
[55] F. H. Séguin *et al.*, Rev. Sci. Instrum. **75**, 3520 (2004).
[56] R. Florido, R. C. Mancini, T. Nagayama, R. Tommasini, J. A. Delettrez, S. P. Regan, and B. Yaakobi, Phys. Rev. E **83**, 066408 (2011).
[57] R. Florido, R. C. Mancini, T. Nagayama, R. Tommasini, J. A. Delettrez, and S. P. Regan, Phys. Plasmas **21**, 102709 (2014).
[58] T. Nagayama, R. C. Mancini, R. Florido, D. Mayes, R. Tommasini, J. A. Koch, J. A. Delettrez, S. P. Regan, and V. A. Smalyuk, Phys. Plasmas **21**, 050702 (2014).
[59] J. T. Larsen and S. M. Lane, J. Quant. Spectrosc. Radiat. Transfer **51**, 179 (1994).
[60] G. Maynard and C. Deutsch, Phys. Rev. A **26**, 665 (1982).
[61] G. Zimmerman, LLNL Report No. UCRL-JC-105616, 1990 (unpublished).
[62] Here it is assumed that the ion-ion stopping power is negligible compared to the ion-electron stopping power. This is valid if $V_i \gg V_{\mathrm{Thi}}$, where V_{Thi} is the ion thermal velocity.
[63] The energy loss of the DD triton is in agreement with the BPS theory, which was not the case reported in previous work [47]. The DD-triton energy loss was reconciled with theory by accounting for the fact that the energy loss explicitly depends on Z_i^2/m_i of the ion (see Supplemental Material [45]) and that the DD-triton energy loss has a small ion-ion component.
[64] Measured with the PXTD diagnostic [49]. The absolute error is ± 50 ps.
[65] Absolute yield error is 5% of the measured value.
[66] Absolute error is ± 20 keV.
[67] $\langle T_i \rangle$ is inferred from the DD-neutron spectrum [50].
[68] $\langle n_e \rangle$, $\langle n_e L \rangle$, and $\langle T_e \rangle$ are the dE/dx-weighted plasma conditions probed by the fusion products. See the Supplemental Material [45].
[69] Shots 78 611 and 78 612 did not measure DD-triton particles and only D ^{3}H α was used to infer $\ln\Lambda_{\mathrm{expt}}$.
[70] Pulse shape is 1 ns square.